AIAA-90-0161
Visualization and Analysis of the Structure of High Reynolds Number Hydrogen-Air Premixed Flames

M.S. Wu, S. Kwon, J.F. Driscoll
and G.M. Faeth
Department of Aerospace Engineering
The University of Michigan, Ann Arbor, MI

28th Aerospace Sciences Meeting
January 8-11, 1990/Reno, Nevada

Visualization and Analysis of the Structure of High Reynolds Number Hydrogen-Air Premixed Flames

M. S. Wu,* S. Kwon*, J. F. Driscoll,† G. M. Faeth**

Abstract

Instantaneous laser light sheet images that describe the orientation and the structure of the reaction surface were obtained within high Reynolds number turbulent premixed flames. The images were analyzed using digital imaging techniques in order to statistically quantify the degree of wrinkledness of the flame surface caused by turbulence. Measurements were made of the perimeter of the wrinkled flame surface, the variance of the flame position, and, in some cases, the fractal dimension of the flame surface. The two types of flames that were studied were a rim-stabilized flame and a wrinkled spherical flame. The incident turbulence intensity was varied, as was the fuel equivalence ratio.

It was found that as turbulence intensity was increased by approximately a factor of three, the flame wrinkles became more fine-grained; i.e., the wrinkles decreased in size but increased in number. The resulting flame perimeter increases as does the overall turbulent burning velocity. The spatial variation of the flame surface wrinkling within the rim-stabilized flame was quantified as a function of the distance from the rim. In an analogous fashion, the wrinkling of the spherically expanding flame was quantified as a function of time from ignition.

Another factor that is found to affect flame surface wrinkling, in addition to incident turbulence, is the degree of preferential diffusion. Keeping the incident turbulence levels fixed, the degree of preferential diffusion was varied by varying the fuel equivalence ratio, yielding a twofold change in the flame perimeter and overall burning velocity.

Nomenclature

A	surface area
c	reaction progress variable
C	empirical constant
d	burner exit diameter
D_2	fractal dimension of a line
D_3	fractal dimension of a surface
ℓ	integral length scale
ℓ_K	Kolmogorov length scale
$\dot{m}$	reactant mass flow rate
P	perimeter
r	radial distance
Re	Reynolds number
S_L, S_T	laminar and turbulent burning velocity
$S_{T,o}, S_{Teff}$	effective turbulent burning velocity
u	streamwise velocity
x	streamwise distance
δ	reaction sheet thickness
ε	length increment
ν	kinematic viscosity
ρ	density
ϕ	fuel equivalence ratio
ω	average reaction rate
Subscripts	
avg	mean exit condition
c	centerline
L	laminar
R	reactant
T	turbulent
o	initial condition
Superscripts	
$\bar{()}$	time-averaged quantity
$\bar{()}'$	time-averaged root-mean-squared fluctuating quantity

Introduction

The recent development of methods to visualize the structure of a flame sheet[1-5] has made it possible to answer certain fundamental questions concerning turbulent premixed flames. One such question is whether or not there is a universal way by which turbulence wrinkles and thus elongates a flame sheet. Simple analyses by Damkohler[6] have assumed that flame wrinkling depends only on the local turbulence properties ahead of the flame sheet; similarly, many previous experimental studies have defined an overall turbulent burning velocity that is a single value that is associated with a given flame. Attempts to correlate the overall turbulent burning velocity measured for flames having very different geometries and stabilization mechanisms have been less than successful.[7,8]

A different and more realistic concept is that a turbulent premixed flame has a spatially varying structure that is not universal but depends on boundary conditions such as those imposed at the flame stabilization location. This concept implies that numerical simulation of premixed flames should correctly simulate, for example, the way in which the wrinkling of a rim-stabilized flame increases with distance from the stabilizing rim. This concept also implies that there is no reason why an overall turbulent burning velocity defined for one geometry, such as a rim-stabilized flame, should correspond to that of another geometry, such as a wrinkled spherical flame. There may be some similarities in the way the flame surface area is affected by turbulence, but spatial and temporal resolved measurements of flame structure are needed to identify such similarities. Even rim-stabilized and rod-stabilized flames can have different structure because the latter "V"-shaped flame consists of two flames, each of which accelerates hot gases toward the centerline and tend to limit the extent of oscillations on the other side of the flame. The

* Graduate Assistant, Aerospace Engineering.
† Associate Professor, Aerospace Engineering, Member, AIAA.
** Professor, Aerospace Engineering, Fellow, AIAA.

flame brush of a rod-stabilized flame thus is typically thinner than that of a rim-stabilized flame.[9,10] By comparison, the structure of non-premixed turbulent flames always has been recognized to be geometry-specific rather than universal in nature. Prediction of non-premixed flame properties requires that the entire flowfield and boundary conditions be considered.

The purpose of the present study is to measure how the flame surface structure varies in space and in time within two types of premixed flames: rim-stabilized and spherical. In the rim-stabilized flame, the degree of wrinkledness is measured as a function of the distance from the rim. A fan-stirred bomb was used to study a wrinkled spherical flame, where the degree of wrinkledness is quantified as a function of time from ignition. Hydrogen-air flames were studied because they are of interest for several advanced propulsion and metal-cutting applications. The incident turbulent velocity fluctuation ($\bar{u}'$) normalized by the laminar burning velocity (S_L) was varied by approximately a factor of three for both types of flames. The statistical information generated by the present study can be used to assess new numerical simulations of premixed flame structure that are being developed. Previous simulation work has been published by Ashurst,[11] Pope,[12] and Borghi.[13]

It is noted that the concept of a turbulent burning velocity is a useful concept as long as the local turbulent burning velocity, denoted S_T, is differentiated from the overall turbulent burning velocity ($S_{T,o}$). S_T is unambiguously defined as $\dot{m}/(\rho_R A_o)$ where $\dot{m}$ is the mass per second of reactants consumed, A_o is the area of the surface that defines the mean flame position, and ρ_R is the gas density of the reactants. Damkohler[6] applied the concept of mass conservation to show that:

$$S_T/S_L = (A_T \sigma_T \omega_T) / (A_o \delta_o, \omega_o) \qquad (1)$$

where S_L is the laminar burning velocity and A_T is the average surface area of the wrinkled flame within the projected region defined by the area A_o of the mean flame surface. The quantity δ_T/δ_o is the ratio of the average reaction sheet thickness to that of a laminar flame. The quantity ω_T/ω_o is the ratio of the average reaction rate within the reaction volume to that of a laminar flame. Damkohler's assumption that δ_T/δ_o and ω_T/ω_o are unity will be violated if sufficient levels of flame stretch are present.[14] In general, the normalized flame surface area A_T/A_o may vary in space and will depend on $\bar{u}'/S_L$ and the fuel equivalence ratio ϕ which affects preferential diffusion. The magnitude of the integral scale and the degree of isotropy of the incident turbulence also are believed to affect A_T/A_o.

Thermo-diffusive instabilities have been shown to affect flame structure in laminar environments and in low intensity turbulent flows.[1] Clavin and Williams[15] have studied these effects using asymptotic analysis. Turbulent deflections of the flame surface were found to be enhanced for unstable conditions and were damped out for stable conditions. Recent work by the present authors[16] demonstrates that the structure of a hydrogen-air flame is significantly affected by preferential diffusion even at relatively high Reynolds numbers. However, for every fuel type chosen, there is one equivalence ratio that results in neutral conditions that are neither stable nor unstable. Measurements were obtained in the present study at stable, unstable and neutral conditions with the realization that the latter conditions are most amenable to numerical simulation.

Experimental Methods

Rim-Stabilized Flame

Figure 1a is a sketch of the rim-stabilized flame burner. A coaxial design was used, consisting of an inner round-jet burner having a diameter of 11 mm and a tube length-to-diameter ratio of 50, to yield nearly fully-developed turbulent pipe flow at the burner exit; and an outer burner having a diameter of 58 mm with the outer flame stabilized much like a flat-flame burner above a bed of beads and screens. The outer burner only served to provide a hot environment for the jet flame: all measurements were limited to the jet flame of the inner burner. The burners operated at atmospheric pressure with combustion products removed by a hood whose inlet was 1 m above the burner exit. Instruments were mounted rigidly; therefore, the burner was traversed in the radial (positioning accuracy of 10 μm) and vertical (positioning accuracy of 1000 μm) directions to measure flame structure.

Hydrogen (99.95% purity) was supplied from commercial cylinders while dry air (dewpoint less than 240 K) was obtained from laboratory supplies. All gas flow rates were measured with rotameters, yielding a maximum uncertainty of fuel-equivalence ratios less than 12% at $\phi = 0.3$ with proportionately lower values at higher fuel-equivalence ratios. The gases were mixed in a manifold and then flowed through long lines (length-to-diameter ratios of ca. 400) to achieve uniform mixtures at the burner inlets. In order to control flashback, which was problematical due to the high flame speeds of hydrogen/air mixtures, flame arrestor screens were installed in the reactant lines of both burners at a location of 50 diameters upstream of the burner exit.

Fan-Stirred Bomb

The fan-stirred bomb is described by Groff.[17] It is similar to the arrangement used earlier by Bradley and coworkers.[7] A sketch of the chamber appears in Fig. 1b. The chamber is quasi-spherical with a volume of 10,600 cc and a 260 mm cross-sectional diameter at the center. Optical access is provided by two 92 mm diameter quartz windows mounted opposite one another. Turbulence was generated by four fans (8 bladed, blade diameter of 135 mm, pitch of 45° located at 90° intervals around the periphery of the vessel). The fans directed their flow toward the center of the vessel and operated at rotational speeds up to 2400 rpm.

The hydrogen and air sources were the same as the jet flame experiments. The proper partial pressures of hydrogen and air were mixed together using the fans and the flame was spark ignited at the center of the vessel using electrodes extending from the top and bottom. The spark gap was roughly 3 mm while the sparks had a duration of 0.5 ms and stored energies of 0.3 mJ.

Fansler[18] measured the properties of the turbulent field produced by the fans using laser velocimetry. The turbulence is nearly isotropic over a region having a diameter of 50 mm at the center of the vessel. Mean velocities are negligible while velocity fluctuations vary linearly with fan speed over the present test range (0.44 m/s at 600 rpm and 0.84 m/s at 1200 rpm) — relatively independent of pressure. Hot-wire measurements during the present investigation confirmed these results at atmospheric pressure — within experimental uncertainties.

Flame Imaging and Analysis

Flame structure was visualized by adding oil drops of nominal diameter of ca. 1 μm to the reactants using a TSI 9306 atomizer. Oil drops of this diameter disappear at the flame surface.[1-5] The drops are illuminated by a 200 μm thick laser light sheet created using a Candela pulsed dye laser and two cylindrical lenses. The laser provides 0.6 J of light at 514.5 nm during a 1 μs pulse duration. Scattered laser light was collected using an 85 mm focal length f1.2 camera lens and a standard 35 mm camera which has its flash synchronization output wired to trigger the laser pulse. To eliminate flame radiation and oil droplet thermal radiation, a 10 nm interference filter was placed in front of the camera lens and the camera shutter duration was set to 8 ms. Each 5 inch by 7 inch photograph obtained was digitally analyzed using an MTI 65 Vidicon camera. Images were processed using a Gould FD 5000 Image Analyzer and an IBM-AT/clone computer. Camera resolution is 1024 × 512 pixels and the typical length of the photographed flame image is 70 mm; thus the spatial resolution of the imaging measurements is 1000 pixels per flame length or 70 μm per pixel.

Test Conditions

The rim-stabilized flame was operated at six different test conditions; two values of $\bar{u}'/S_L$ were chosen, 0.9 and 2.5, and three values of fuel equivalence ratio, ϕ: 0.8, 1.8 and 3.6. For ϕ = 1.8 the hydrogen-air flame has its maximum laminar burning velocity and this is neutral with respect to preferential diffusion effects. Values of ϕ = 0.8 and ϕ = 3.6 were chosen because the laminar burning velocity S_L is the same for these two cases. However the ϕ = 0.8 flame is diffusionally unstable and the ϕ = 3.6 flame is diffusionally stable. Therefore any observed differences in flame structure, perimeter or turbulent burning velocity can be attributed to preferential diffusion effects.

Typical conditions plotted in Fig. 2 to show the various regimes in which the rim-stabilized flame conditions occur. The present flames having $\bar{u}'/S_L$ equal to 0.9 fall into the wrinkled continuous flame sheet regime and have reaction zones significantly thinner than the Kolmogorov scale of the turbulence. The flames that have $\bar{u}'/S_L$ equal to 2.5 are more likely to have local islands of reaction zones in addition to a very wrinkled continuous flame sheet. Only for the leanest flames (ϕ = 0.3), that were not studied in the present work, could flames be stabilized that had the calculated Kolmogorov thickness smaller than the reaction zone thickness.

The fan-stirred bomb was used to visualize flames at four different conditions. Four values of fan speed were chosen to give $\bar{u}'/S_L$ equal to 0.0, 0.29, 0.48 and 0.65. Only one fuel equivalence ratio was chosen, namely ϕ = 1.8 which is diffusionally neutral. In addition, nitrogen was added to the air so that the oxygen fraction of the oxygen-nitrogen mixture was decreased from 22% (air) to 15%. The nitrogen was added to reduce the laminar burning velocity and thus increase $\bar{u}'/S_L$ in order to increase the wrinkling of the flame surface during the available test time. The spherical flames were all operated at $\bar{u}'/S_L$ less than unity, which is in the wrinkled flame regime of Fig. 2, with turbulent Reynolds number $\bar{u}'\ell/\nu_o$ in the range 0-2500.

Results and Discussion

Rim-Stabilized Flame Structure

Typical photographs of the rim-stabilized flame are shown in Fig. 3 for the six selected test conditions. It is observed that the three flames that experience higher initial turbulence levels ($\bar{u}'/S_L$ = 2.5) have a much finer-grained structure than the three flames for which $\bar{u}'/S_L$ = 0.9. The difference in structure is believed to result from the fact that the flames having the larger value of $\bar{u}'/S_L$ are subjected to vortices in the incident flow that are nearly three times stronger than those in the flows for which $\bar{u}'/S_L$ is 0.9. If $\bar{u}'/S_L$ could be increased without limit and flame strainout did not occur, the premixed flame would conceptually be "mixing-limited." That is, the flame surface would follow the contour of a passive scalar, the surface shape would be determined entirely by the incident flow field and the self-propagation of the surface would be negligible. At the hypothetical mixing-limited, zero strainout limit, it is expected that the spectrum of flame wrinkle sizes and incident eddy sizes would be highly correlated.

The integral scale of the incident turbulence (in the radial direction) for all six cases in Fig. 3 is approximately one-eighth of the burner diameter, based on the pipe flow measurements of Laufer.[19] The Kolmogorov scale is estimated to be one-three hundreth of the burner diameter (i.e., 30 μm) for the case $\bar{u}'/S_L$ = 0.9. This is based on the conventional relation that states that the Kolmogorov scale varies with the Reynolds number, based on turbulent properties, to the minus 3/4 power.[19] Therefore it is concluded that the wrinkles observed in Fig. 3 for the $\bar{u}'/S_L$ = 0.9 case do not correspond to the sizes of eddies in the incident flow. In fact, most of the flame wrinkles are larger than the integral scale of the incident turbulence. The wrinkle size appears to increase as the distance from the rim increases.

A second parameter that has a major effect on flame structure is the fuel equivalence ratio ϕ. The values of $\bar{u}'$, $\bar{u}_o$, S_L and the ratio $\bar{u}'/S_L$ are exactly the same for the ϕ = 0.8 case and for the ϕ = 3.6 case for $\bar{u}'/S_L$ = 0.9. The same is true for the ϕ = 0.8 and ϕ = 3.6 cases for $\bar{u}'/S_L$ = 2.5. The observed differences in flame structure, flame length, and flame perimeter, as discussed below, between the ϕ = 0.8 and ϕ = 3.6 cases are attributed to preferential diffusion.[6,15]

The first flame shown in Fig. 3 represents the unstable case (ϕ = 0.8); the flame wrinkles appear to be more numerous and have more of a cusped-like shape than the wrinkles observed for the diffusionally stable case (ϕ = 3.6). The shorter flame length associated with the unstable (ϕ = 0.8) case indicates that the flame has more surface area with which to consume the reactants. At $\bar{u}'/S_L$ = 2.5 the unstable (ϕ = 0.8) flame also is shorter than the stable (ϕ = 3.6) flame.

For each of the six conditions shown in Fig. 3, thirty flame images were digitized and analyzed. The mean flame shape is shown in Fig. 4. These results confirm, in a statistical sense, that the stable flame (ϕ = 3.6) is significantly longer than the unstable (ϕ = 0.8) flame. The variance in the flame radial location, $\bar{r}'$, is shown in Fig. 5. The results show that the initial slope of the ϕ = 0.8 curve is significantly less than the initial slope of the ϕ = 3.6 curve. This implies that the variance of flame location, $\bar{r}'$, which is a measure of flame brush thickness, increases less rapidly in the axial direction for the stable case (ϕ =

3.6) than for the unstable case. The differences in the slopes observed in Fig. 5 can be explained by the known mechanism by which a diffusionally stable flame damps out the disturbances caused by turbulence.

Another measure of the local wrinkledness of the flame surface is the normalized flame perimeter P_T/P_L which is plotted in Fig. 6. To obtain this quantity, the x axis was divided up into segments, each having a length of 7 mm. In each segment, the perimeter of the wrinkled digitized image, as shown in Fig. 3, was computed and is denoted P_T. The perimeter of the mean flame coordinates, as shown in Fig. 6, also was computed for each segment and is denoted P_L. Figure 6 quantifies how the quantity P_T/P_L varies with the distance from the rim. For the diffusionally stable flame, the flame perimeter grows much less rapidly as a function of x/d than does the perimeter of the unstable case. This is consistent with the previous results shown in Figs. 3-5.

One other method that was used to quantify the mean flame length was single-point Rayleigh scattering. The system used is described in Ref. 16. The gas density was measured along the burner centerline and the profile of mean reactedness ($\bar{c}$) was determined. Results are shown by the circular symbols in Fig. 7. The mean flame length is defined as the axial location where ($1-\bar{c}$) decreases to a value of 0.5. The flame lengths deduced from Fig. 7 agree with the trends described previously by the data in Fig. 4. That is, the open symbols in Fig. 7, for example, indicate that the lean flame (ϕ=0.8), which is diffusionally unstable, is significantly shorter than the rich flame (ϕ = 3.6) which is diffusionally stable. Each symbol in Fig. 7 represents the ensemble average of 4096 single-point samples.

Overall Turbulent Burning Velocity

The overall turbulent burning velocity ($S_{T,o}$) is a useful measure of the rate at which the reactants are consumed in a flame. $S_{T,o}$ is defined as $\dot{m}/(\rho_R A_o)$, where $\dot{m}$ is the mass per second of reactants consumed, ρ_R is the gas density of reactants, and A_o is the area of the surface defined by the mean flame position. For a rim-stabilized flame, $S_{T,o}$ is useful because it quantifies the expected height of the flame tip for a given mass flow rate. In the present study, an effective conical surface was defined that has a base diameter equal to the burner exit diameter and a height equal to the measured flame height defined by the $\bar{c}$ = 0.5 location in Fig. 7.

The overall turbulent burning velocity, $S_{T,o}$ was then defined as the mean velocity normal to this surface, assuming that the mean streamwise velocity was the same as at the burner exit. This assumption is justified because all flames for which $S_{T,o}$ was computed lie within the potential core of the jet, where the velocity does not vary in the axial direction, as shown later. This method of using the mean flame location to define an effective angle between the turbulent flame and the incoming reactant velocity has been commonly used to determine turbulent burning velocity.[8,9,20,21]

The resulting effective turbulent burning velocities are illustrated in Fig. 8. The values of S_L used for these correlations were obtained from Andrews and Bradley.[22] The measurements illustrated indicate that effective turbulent flame speeds fall on two branches: a neutral-unstable branch involving ϕ = 0.8, 1.0 and 1.8, and a stable branch involving ϕ = 3.57. The stable branch has substantially less response to increased turbulence levels (i.e., smaller slope) than the neutral-unstable branch. Furthermore, even within the neutral-unstable branch, unstable conditions are somewhat more responsive to increased turbulence levels than the neutral condition. These trends clearly imply that diffusive-thermal phenomena retard turbulent distortion of the flame surface for stable conditions (thus yielding lower values of $S_{T,o}$), and to a lesser degree, enhance distortion for unstable conditions (yielding higher values of $S_{T,o}$).

Other measurements in the literature yield similar behavior. For example, Abdel-Gayed et al.[23] measured turbulent burning velocities of hydrogen/air mixtures at various ϕ using a fan-stirred bomb. When these measurements are correlated in the same manner as Fig. 9, two branches are also observed: results for ϕ = 0.42-1.58 yielding an unstable branch, and results for ϕ = 3.57 yielding a stable branch having a smaller response to increased turbulence levels. Abdel-Gayed et al.[23] attribute the reduced response for ϕ = 3.57 to quenching, however, since S_L for this condition actually exceeds values for some of the conditions in the unstable branch, preferential diffusion phenomena must play an important role in this behavior.

Liu and Lenze[24] measured turbulent burning velocities of CH_4-H_2/air mixtures stabilized at a stagnation point. They also find that rich flames have reduced response to increased turbulence levels in comparison to lean flames but do not propose a reason for this behavior.

Taken together, these results suggest that diffusive-thermal phenomena influence the rate of propagation of turbulent flames at all but neutral conditions for high Reynolds numbers as well as low Reynolds numbers. Stable conditions tend to reduce distortion of the flame surface by the turbulence and, to a lesser degree, unstable conditions tend to enhance distortion of the flame surface by turbulence. These effects may explain past difficulties in obtaining correlations of turbulent flame speeds along the lines of Fig. 8, as well as reliable models of turbulent combustion for premixed flames. Finding a rational way to incorporate preferential diffusion effects into methods of estimating turbulent flame speeds has important implications, e.g., most practical premixed turbulent flames, like those of spark ignition automotive engines, involve reactant systems having widely varying mass diffusivities and operate at stable conditions where diffusive-thermal effects are likely to significantly retard distortion of the flame surface by turbulence.

Laser velocimeter measurements of the axial velocity along centerline of the flame are shown in Fig. 9. The purpose of these measurements is to determine if the rim-stabilized flame exists within the potential core of the jet burner. The square symbols in Fig. 9 indicate the flame tip location, as deduced from Fig. 7. The flame tip is seen to occur in the range of x/d between 2 to 10 except for one case (Re = 40,000, ϕ = 3.6). In all cases, the potential core length, as defined by a 10 percent dropoff in the axial velocity, is seen to exceed 10 d. Therefore, it is concluded that in all but one case, the flames exist within the potential core.

In the core region, the incident turbulence that wrinkles the flame is well-defined pipe flow turbulence and not the shear layer turbulence that is generated outside of the core. The radial profiles of axial velocity were measured at the burner tube exit; results appearing in Fig. 10 show that the profiles of $\bar{u}_o$ and $\bar{u}'$ agree with well-established turbulent pipe flow profiles.

Wrinkled Spherical Flame Structure

Typical images of the wrinkled spherical flame that was generated in the fan-stirred bomb are shown in Fig. 11. The light sheet and oil drops used were similar to those used for the rim-stabilized flame. The fuel equivalence ratio was selected to be 1.8 in order to maintain diffusionally neutral conditions. Nitrogen was added so that the oxygen-nitrogen gas mixture used was 15% oxygen. Figure 11 shows that the turbulence levels that were chosen ($\bar{u}'/S_L$ = 0.47 and 0.94 in this case) are sufficient to severely wrinkle the flame during the test times available. The flame wrinkles are not strongly cusped in the neutral case shown in Fig. 11; however, if diffusionally unstable conditions are chosen, the cusps become more prominent and then the flame has a cellular appearance.[16]

To quantify the structure of the wrinkled spherical flames, one fuel equivalence ratio (ϕ = 1.8) was used, four turbulence levels ($\bar{u}'/S_L$) were chosen, and at least four different times from ignition were selected. For each of these conditions, six photographs were obtained and analyzed. The equivalent mean radius is defined as the radius of a circle that has the same area as that enclosed by the wrinkled flames. Ensemble-averaged results are shown in Fig. 12; it is seen that the equivalent mean radius increases nearly linearly with time in the period when measurements were made.

The wrinkled structure of the flame was quantified by the variance in the fluctuation of radial position ($\bar{r}'$) and by the fractal dimension of the flame surface. Fluctuations of radial position were obtained by selecting 60 angular positions and computing the ensemble average of the root-mean-squared difference between flame radius and the mean equivalent radius. The fractal dimension of the two-dimensional curve that is shown in the flame photographs of Fig. 11 was computed in the following manner. A length scale ε is chosen to measure the perimeter P of the curve. About a chosen starting position on the curve, a circle is drawn having radius ε. This circle will intersect the curve at some point, about which another circle of radius ε is drawn. When the sequence of circles extends to the end of the curve, the perimeter P is computed by counting the number of circles in the sequence and multiplying this number by ε. The process is repeated for a range of values for ε. This conceptual process was done numerically by computing the coordinates of the locus of points on each circle. The 2-D fractal dimension D_2 is defined by the following relation:[4,5]

$$P = C\,\varepsilon^{2-D_2}$$

where C is a constant. The 3-D fractal dimension D_3 is D_2+1 if the surface wrinkles are isotropic;[4] i.e., if the computed value of D_2 is independent of the orientation of the laser light sheet with respect to the flame surface.

Computed values of $\bar{r}'$ and D_3 are shown in Fig. 13. Both D_3 and $\bar{r}'$ are seen to increase linearly with mean flame radius, which is proportional to time from ignition. Figure 13 quantifies the increase in flame wrinkling that occurs as the initial turbulence level is increased. Inspection of Fig. 13 reveals that as the initial turbulence level ($\bar{u}'/S_L$) is increased, D_3 and $\bar{r}'$ increase, but not necessarily in a manner that is linearly related to ($\bar{u}'/S_L$). The measurements reported in Fig. 13 represent one way to assess the accuracy of numerical simulations of the structure of premixed turbulent flames.

Conclusions

1. The rate at which flame wrinkling increases with distance from the rim of a rim-stabilized flame is quantified. Also quantified is the rate at which a spherically expanding flame wrinkles as a function of time. Parameters that were measured include the flame perimeter, the variance in the radial position of the flame (i.e., the flame brush thickness), and the fractal dimension of the flame surface.

2. As the normalized initial turbulence level ($\bar{u}'/S_L$) is increased, the flame wrinkles become fine-grained; the wrinkles decrease in size but increase in number. Flame perimeter, brush thickness ($\bar{r}'$), and fractal dimension all increase as $\bar{u}'/S_L$ increases, which is consistent with the measured increase in overall turbulent burning velocity.

3. Preferential diffusion has a significant effect on the flame perimeter and on the overall turbulent burning velocity, even at the high Reynolds numbers studied. These flame properties vary by as much as a factor of two, depending on whether the flame is diffusionally stable or unstable. Only for the diffusionally neutral case can numerical simulations properly ignore the effects of preferential diffusion.

Acknowledgement

This research was supported by the Office of Naval Research, Contract No. N00014-87-K-0698, with S. Ramberg serving as Scientific Program Officer. The authors also wish to thank E. G. Groff for many useful discussions and General Motors Research Laboratories for the loan of the fan-stirred bomb.

References

[1]Boyer, L., Clavin, P. and Sabathier, F., "Dynamic Behavior of a Premixed Turbulent Flame Front." *Eighteenth Symposium (International) on Combustion*, The Combustion Institute, Pittsburgh, 1980, pp. 1041-1049.

[2]Chew, T. C., Britter, R. E. and Bray, K.N.C., "Laser Tomography of Turbulent Premixed Bunsen Flames." *Combust. Flame* 75, 165-169, 1989.

[3]Murayama, M. and Takeno, T., "Fractal-Like Character of Flamelets in Turbulent Premixed Combustion." *Twenty-Second Symposium (International) on Combustion*, The Combustion Institute, Pittsburgh, 1988, pp. 551-559.

[4]Mantzaras, J., Felton, P. G. and Bracco, F. V., "Fractals and Turbulent Premixed Engine Flames," *Combust. Flame* 77, 295-310, 1989.

[5]Gouldin, F. C., Bray, K.N.C. and Chen, J. Y., "Chemical Closure Model for Fractal Flamelets." *Combust. Flame* 77, 241-259, 1989.

[6]Lewis, B. and von Elbe, G., *Combustion, Flames and Explosions of Gases*, 2nd edition, Academic Press, New York, 1961, pp. 381-384.

[7]Abdel-Gayed, R. G. and Bradley, D., "Dependence of Turbulent Burning Velocity on Turbulent Reynolds Number and Ratio of Laminar Burning Velocity to R.M.S. Turbulent Burning Velocity." *Sixteenth Symposium (International) on Combustion*, The Combustion Institute, Pittsburgh, 1976, pp. 1725-1735.

[8]Ballal, D. R. "The Structure of a Premixed Turbulent Flame." *Proc. R. Soc. London A 367*, pp. 353-370, 1979.

[9]Driscoll, J. F. and Gulati, A., "Measurement of Various Terms in the Turbulent Kinetic Energy Balance Within a Flame and Comparison with Theory." *Combust. Flame* 71, 131-152, 1988.

[10]Cheng, R. K. and Ng, T. T., "Velocity Statistics in Premixed Turbulent Flames," *Combust. Flame* 52, 185-202, 1983.

[11]Ashurst, W. T., "Vortex Simulation of Unsteady Wrinkled Laminar Flames." *Comb. Sci. and Tech.* 52, 325, 1987.

[12]Pope, S. B. and Cheng, W. K., "Statistical Calculations of Spherical Turbulent Flames." *Twenty-First Symposium (International) on Combustion*, The Combustion Institute, Pittsburgh, 1986, pp. 1473-1481.

[13]Said, R. and Borghi, R., *Twenty-Second Symposium (International) on Combustion*, The Combustion Institute, Pittsburgh, 1988, pp. 569-577.

[14]Law, C. K., "Dynamics of Stretched Flames." *Twenty-Second Symposium (International) on Combustion*, The Combustion Institute, Pittsburgh, 1988, p. 1381.

[15]Clavin, P. and Williams, F. A., "Effects of Molecular Diffusion and of Thermal Expansion on the Structure and Dynamics of Premixed Flames in Turbulent Flows of Large Scale and Low Intensity." *J. Fluid Mech.* 116, 251, 1982.

[16]Wu, M. S., Kwon, S., Driscoll, J. F. and Faeth, G. M., "Turbulent Premixed Hydrogen-Air Flames at High Reynolds Number." *Comb. Sci. and Tech.*, submitted.

[17]Groff, E. G., "The Cellular Nature of Confined Spherical Propane-Air Flames." *Combust. Flame* 48, 51, 1982.

[18]Fansler, T. D. and Groff, E. G., "Turbulence Characteristics of a Fan-Stirred Combustion Vessel."*Combust. Flame*, in press.

[19]Hinze, J. O., *Turbulence*. Section 7-9, Turbulence Quantities in Pipe Flow, p. 520, McGraw-Hill, New York, 1959.

[20]Cheng, R. K. and Ng, T. T., "On Defining the Turbulent Burning Velocity in Premixed V-Shaped Turbulent Flames." *Combust. Flame* 57, 155, 1984.

[21]Dandecar, K. V. and Gouldin, F. C., "Temperature and Velocity Measurements in Premixed Turbulent Flames." *AIAA J.* 20, 652, 1982.

[22]Andrews, G. E. and Bradley, D., "Determination of Burning Velocity by Double Ignition in a Closed Vessel." *Combust. Flame* 20, 77, 1973.

[23]Abdel-Gayed, R. G., Bradley, D., Hamid, M. N. and Lawes, M., "Lewis Number Effects on Turbulent Burning Velocity." *Twentieth Symposium (International) on Combustion*, The Combustion Institute, Pittsburgh, 1984, pp. 505-512.

[24]Liu, Y. and Lenze, B., "The Influence of Turbulence on the Burning Velocity of Premixed CH_4-H_2 Flames With Different Laminar Burning Velocities." *Twenty-Second Symposium (International) on Combustion*, The Combustion Institute, Pittsburgh, 1988, pp. 747-754.

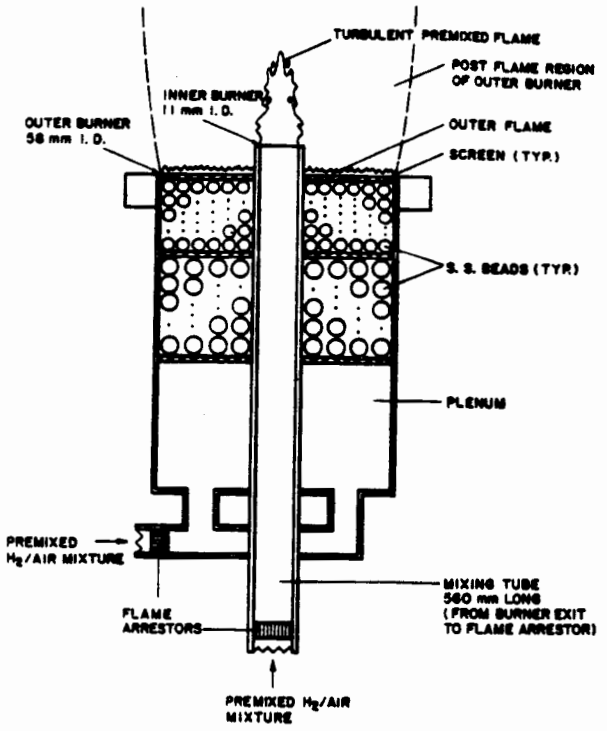

Figure 1a Schematic of the Rim-Stabilized Flame.

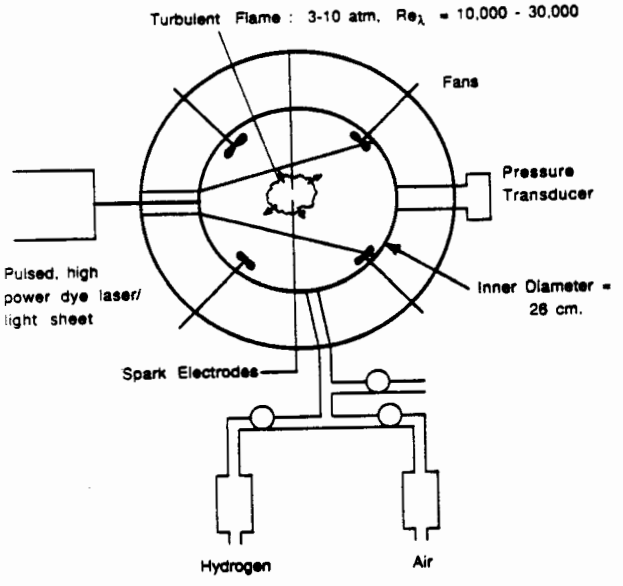

Figure 1b Schematic of the Fan-Stirred Bomb.

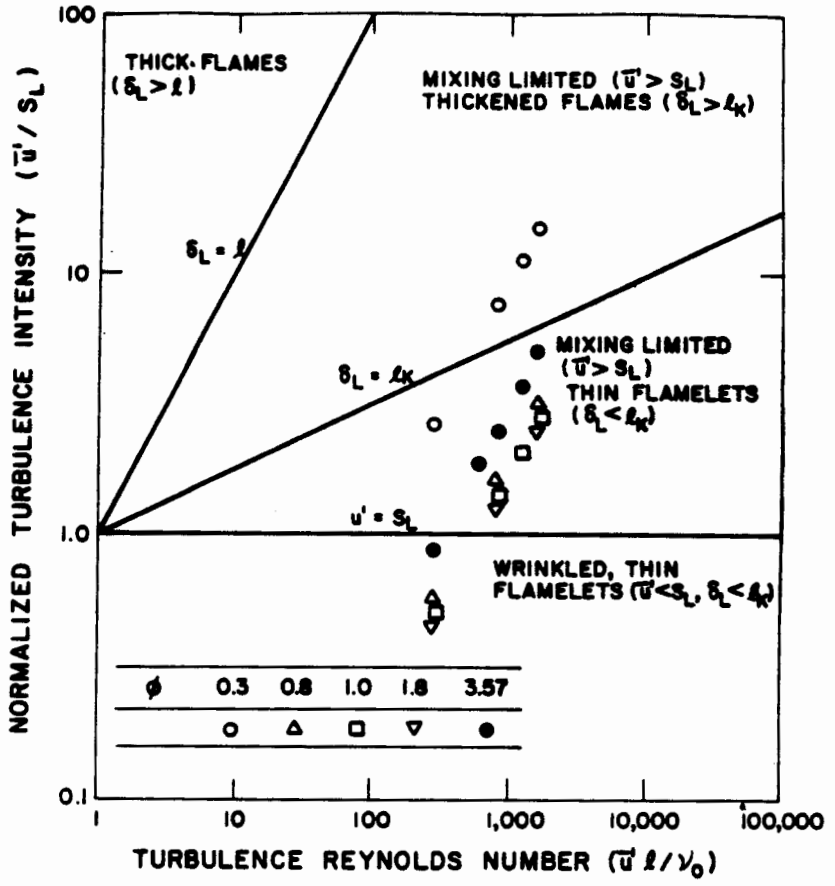

Figure 2 Turbulent Flame Regimes of the Measurements.

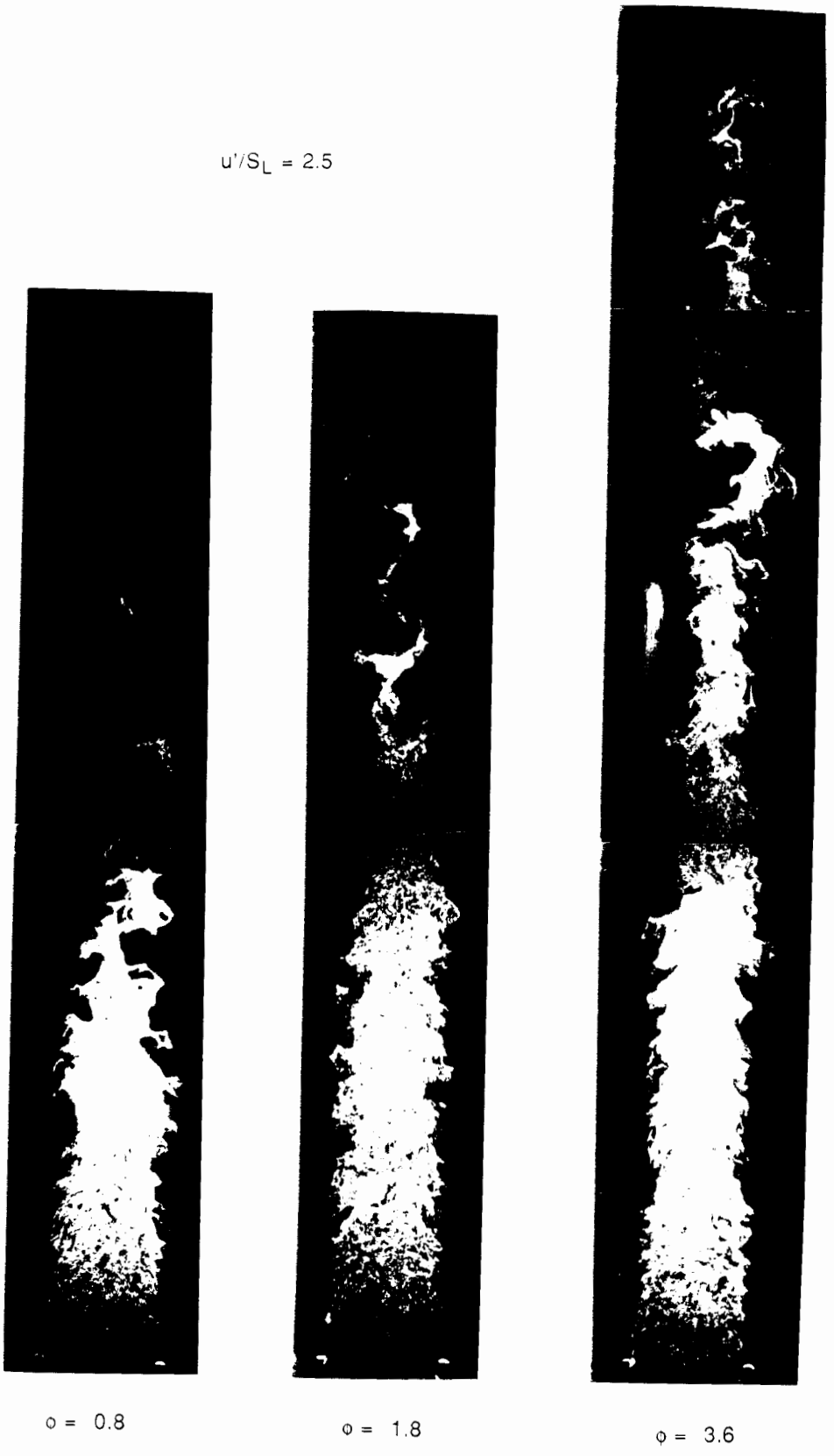

Figure 3. Typical Laser Light Sheet Images of the Rim-Stabilized Flames.

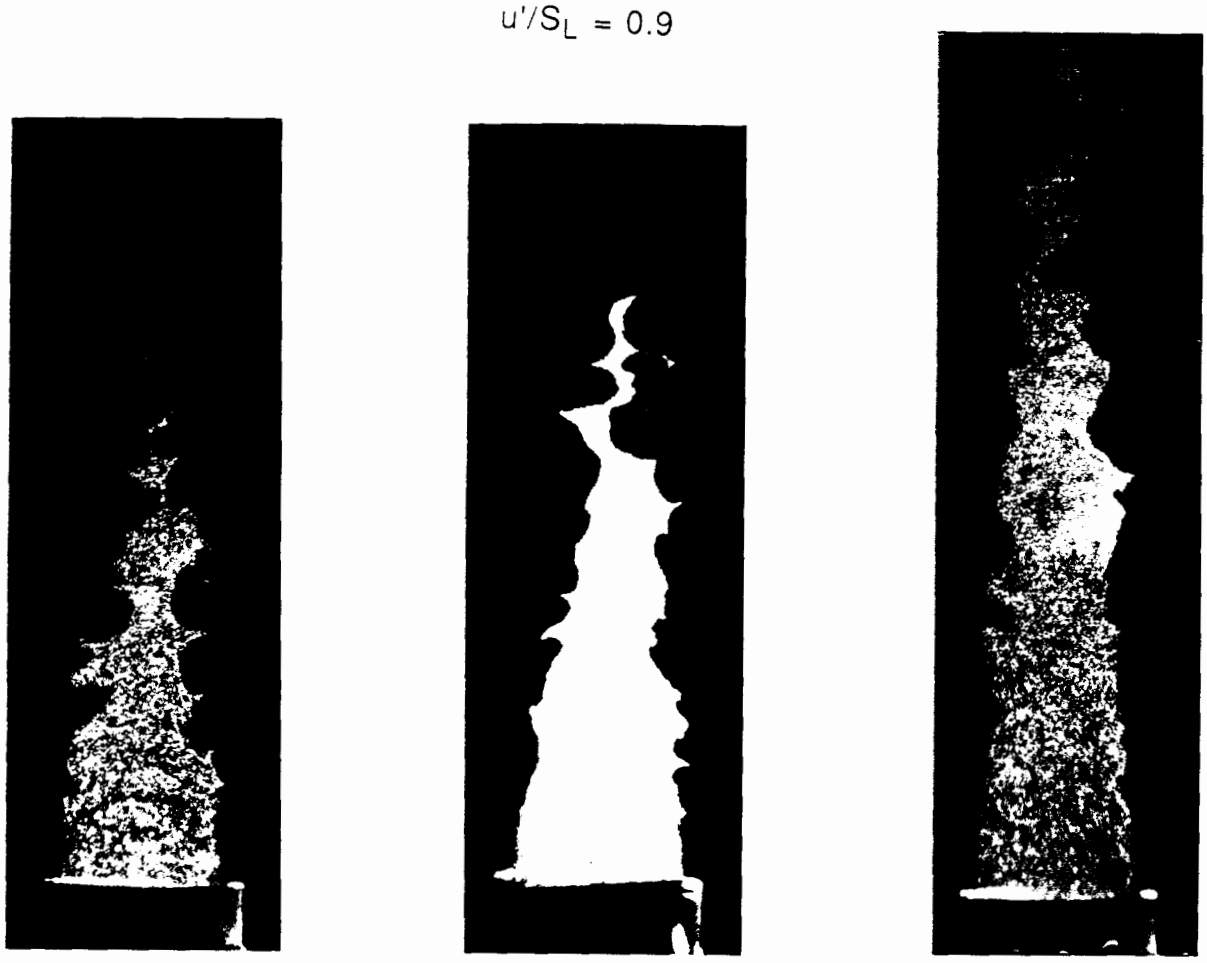

Figure 3. Typical Laser Light Sheet Images of the Rim-Stabilized Flames.

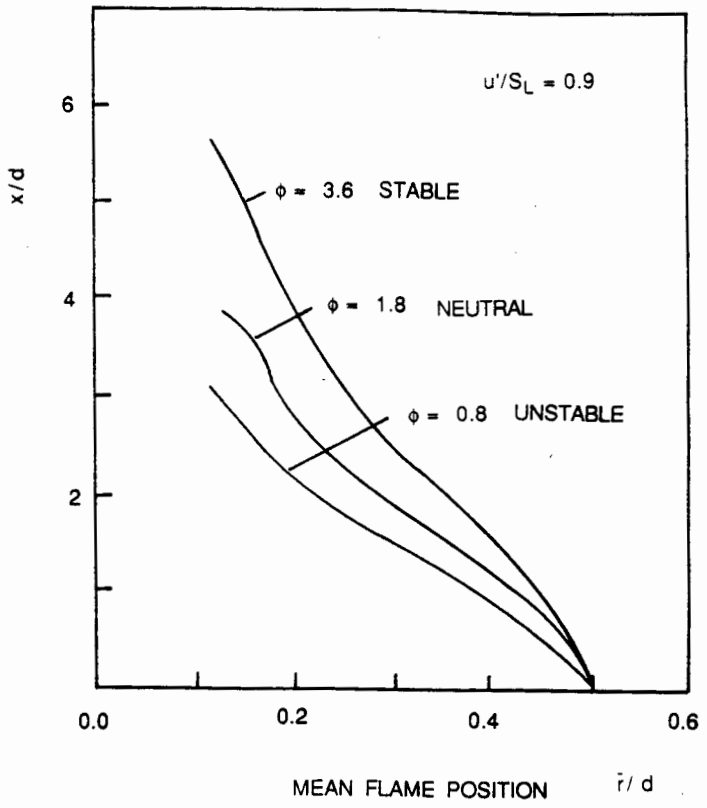

Figure 4. Mean Flame Position for the Rim-Stabilized Flame.

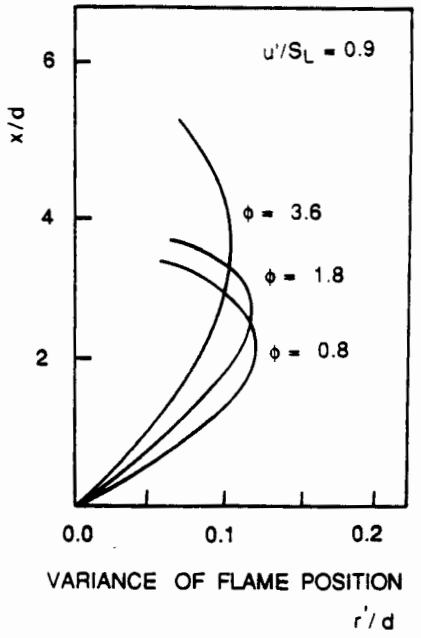

Figure 5. Variance of Flame Location About Its Mean Position.

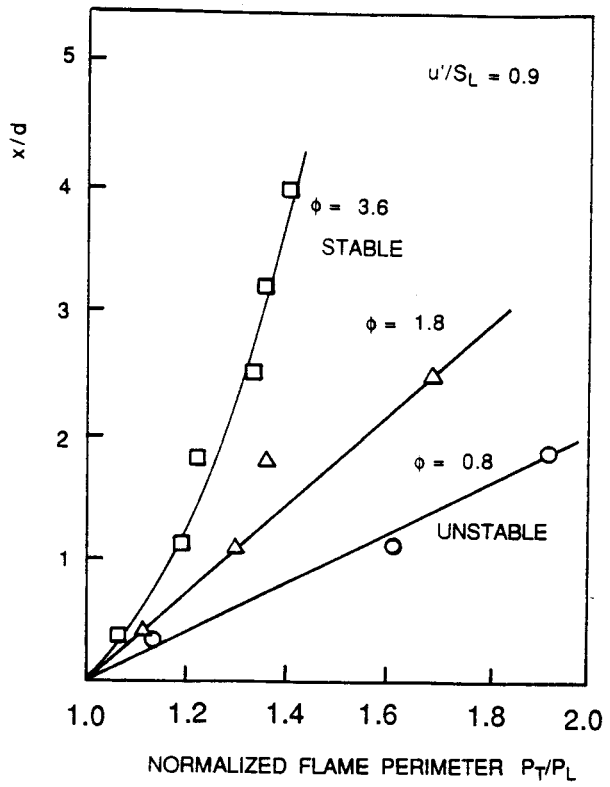

Figure 6. Perimeter of Wrinkled Flame, Normalized By Perimeter of Mean Position of Rim-Stabilized Flame.

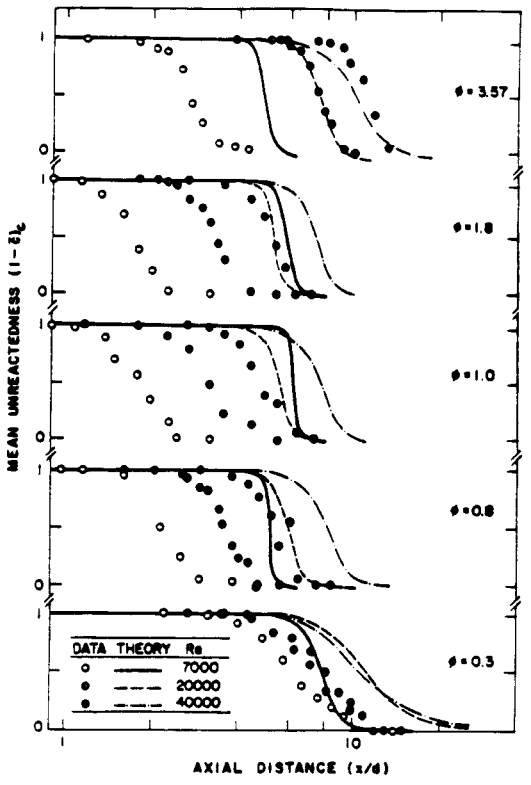

Figure 7. Mean Unreactedness Along Burner Axis, Obtained From Rayleigh Scattering Data.

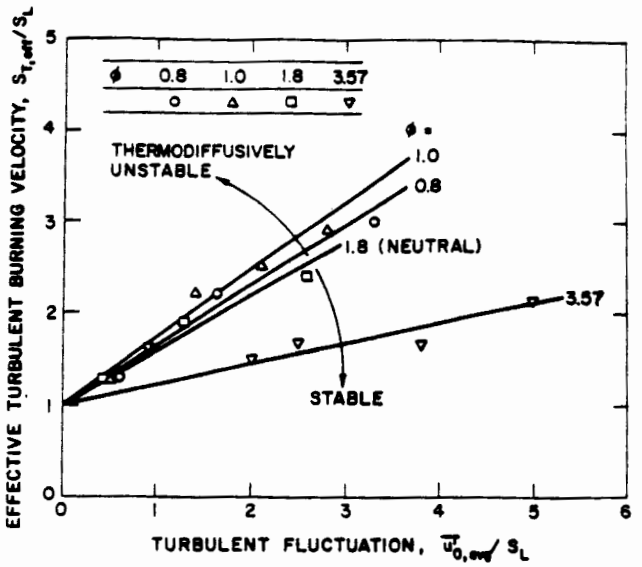

Figure 8. Effective Turbulent Burning Velocity as a Function of Upstream Velocity Fluctuations.

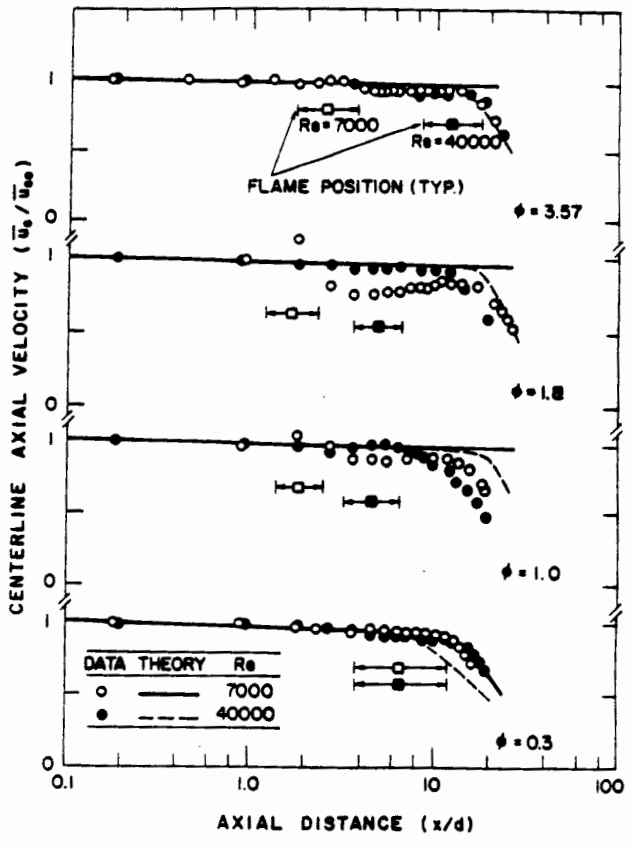

Figure 9. Flame Position Within the Potential Core of the Burner.

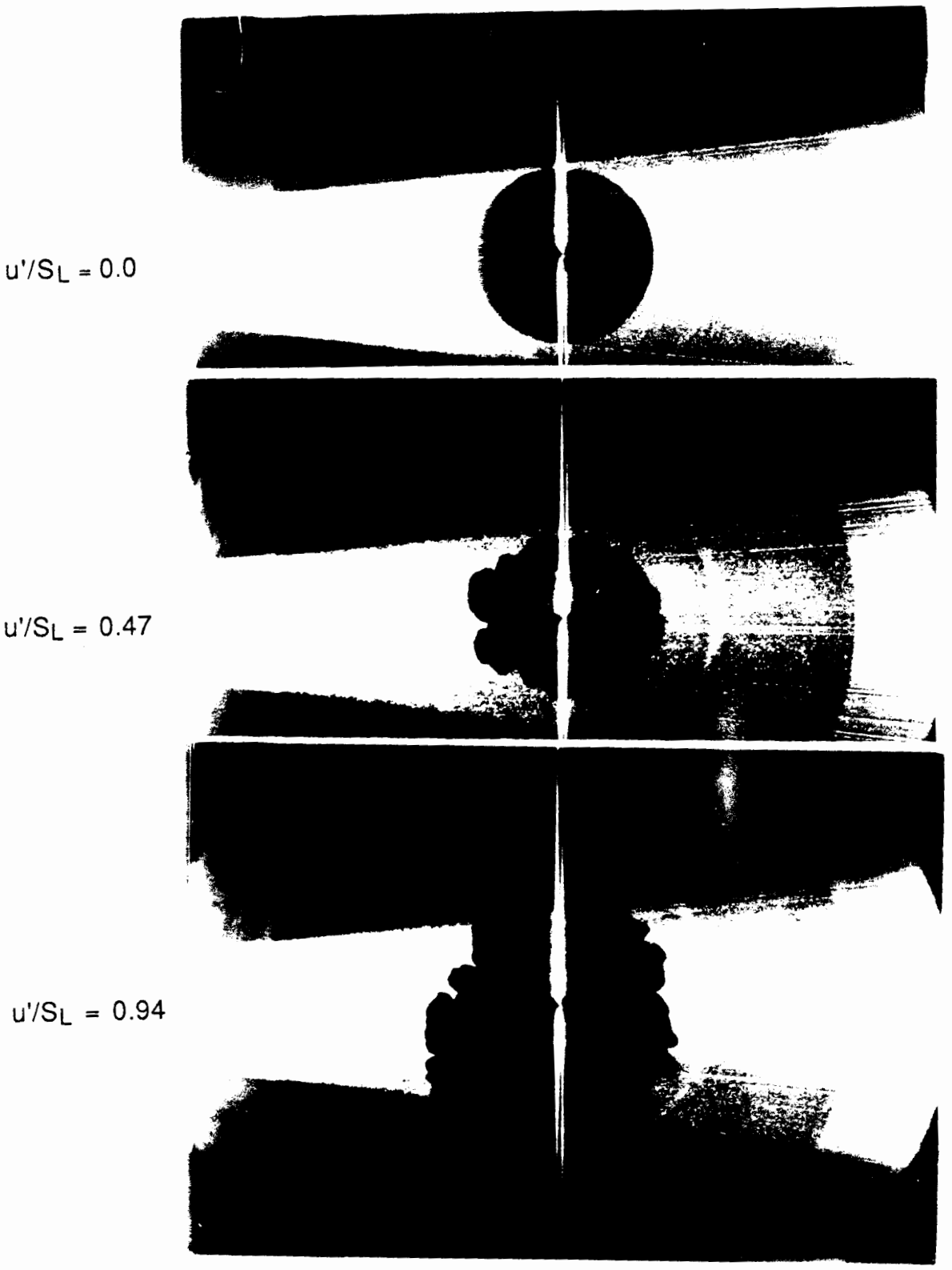

Figure 11. Typical Laser Light Sheet Images of the Flames in the Fan-Stirred Bomb.

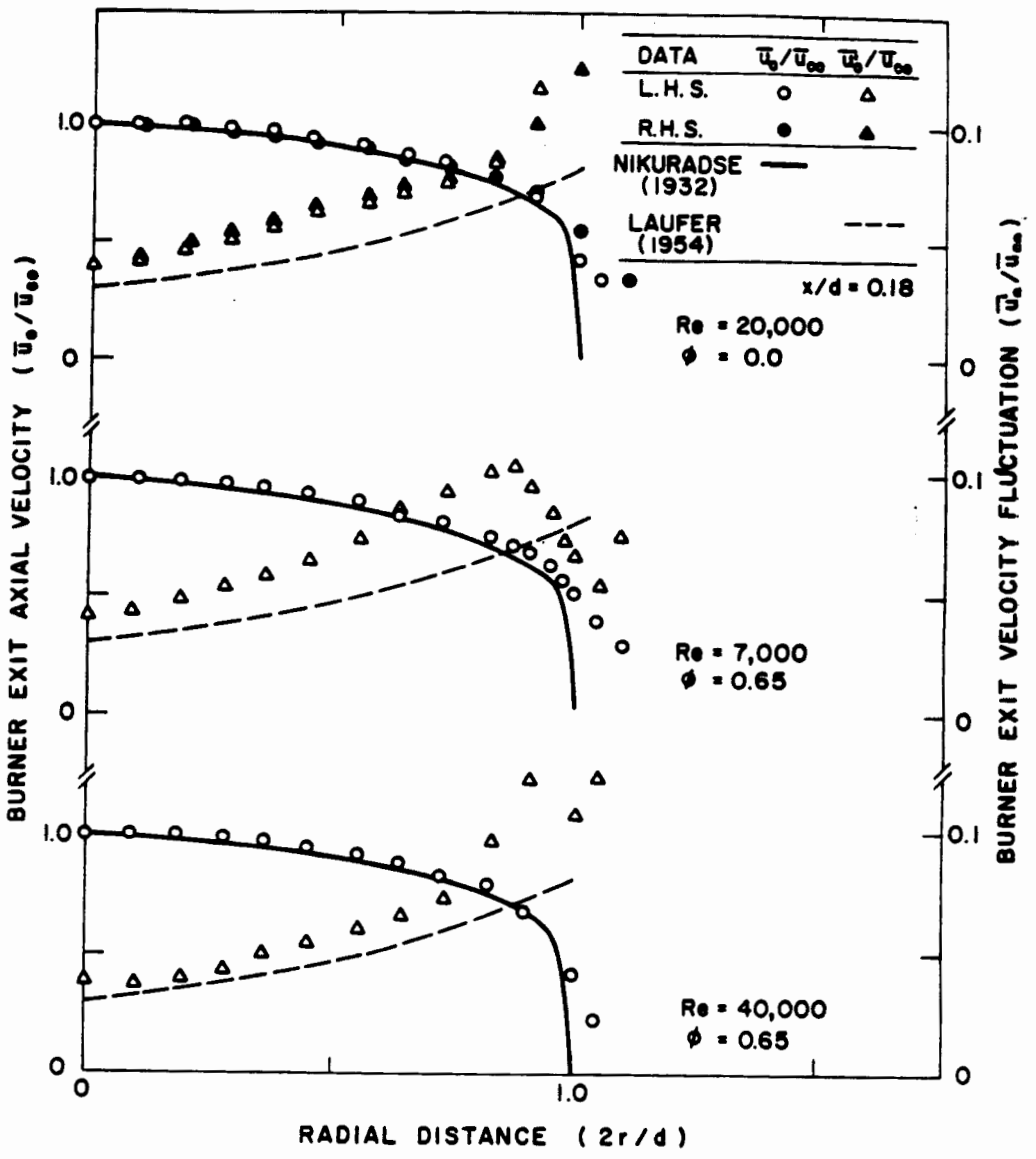

Figure 10. Profiles of initial mean velocity and velocity fluctuations compared with pipe flow profiles of Laufer and Nikuradse

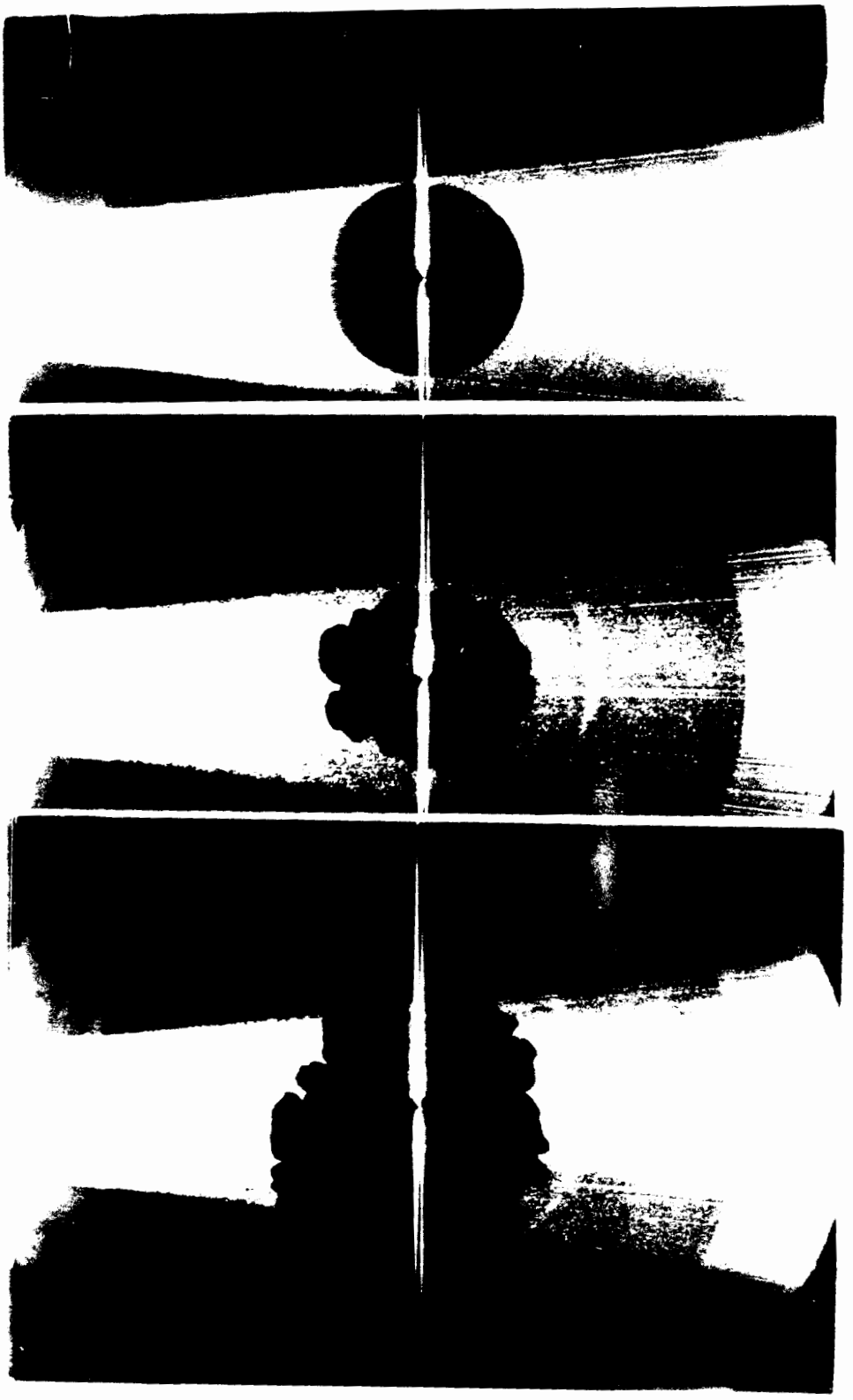

Figure 11. Typical Laser Light Sheet Images of the Flames in the Fan-Stirred Bomb.

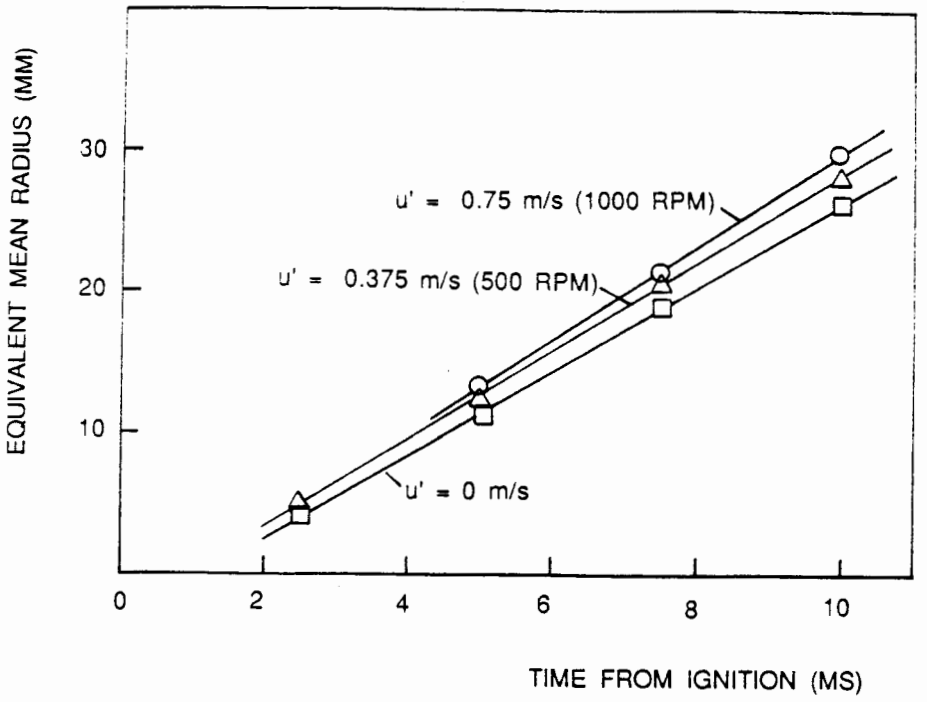

Figure 12. Mean Radius of the Flame in the Fan-Stirred Bomb.

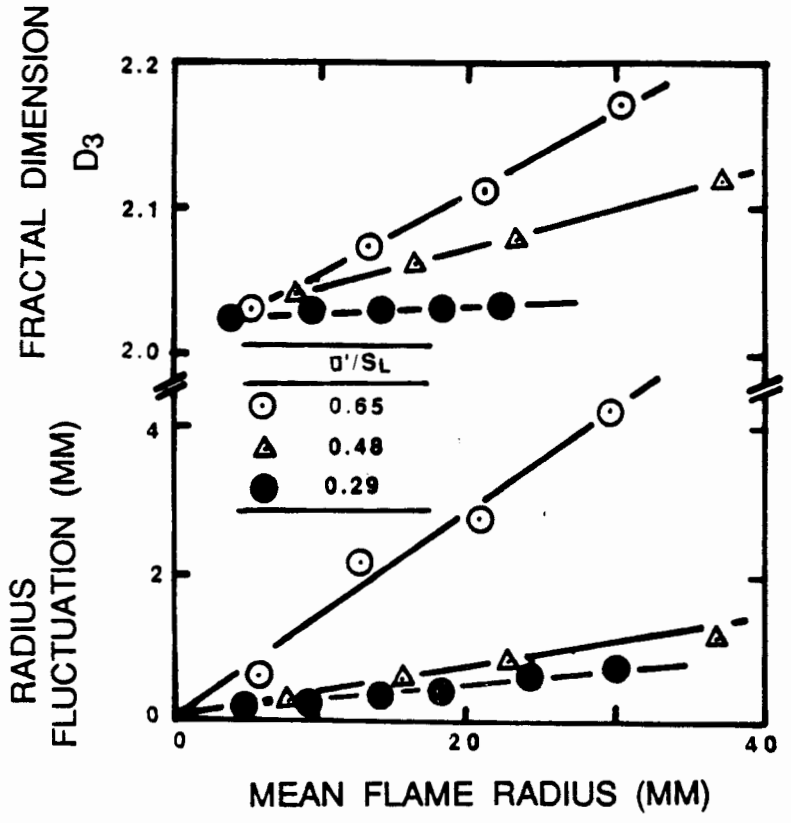

Figure 13. Variance of Flame Position About Its Mean Radius in the Fan-Stirred Bomb, and Fractal Dimension of Flame Images